JAAS

Accepted Manuscript

This is an *Accepted Manuscript*, which has been through the Royal Society of Chemistry peer review process and has been accepted for publication.

Accepted Manuscripts are published online shortly after acceptance, before technical editing, formatting and proof reading. Using this free service, authors can make their results available to the community, in citable form, before we publish the edited article. We will replace this *Accepted Manuscript* with the edited and formatted *Advance Article* as soon as it is available.

You can find more information about *Accepted Manuscripts* in the Information for Authors.

Please note that technical editing may introduce minor changes to the text and/or graphics, which may alter content. The journal's standard Terms & Conditions and the Ethical guidelines still apply. In no event shall the Royal Society of Chemistry be held responsible for any errors or omissions in this *Accepted Manuscript* or any consequences arising from the use of any information it contains.

ROYAL SOCIETY OF CHEMISTRY

www.rsc.org/jaas

Journal Name Journal of Analytical Atomic Spectrometry Dynamic Article Links ►

Cite this: DOI: 10.1039/c0xx00000x

www.rsc.org/xxxxxx

ARTICLE TYPE

Possibilities and analytical properties of the radiofrequency plasma pencil operated in the continual and in the pulsed mode

Lukáš Novosád[a], Aleš Hrdlička[b], Pavel Slavíček[c], Vítězslav Otruba[a] and Viktor Kanický[a]

Received (in XXX, XXX) Xth XXXXXXXXX 20XX, Accepted Xth XXXXXXXXX 20XX

DOI: 10.1039/b000000x

A two-electrodes capacitively coupled plasma jet discharge operated on a symmetrical sinus frequency carrier wave 13.56 MHz in a continual mode and in a pulsed mode is described in this paper. Internally pulsed mode was realised by the frequency modulation by the symmetrical rectangular frequency 22 kHz with duty cycle of 90 %. The pulsed mode has an effect on the electron number densities ranging from 1×10^{14} to 1.2×10^{15} in the pulse mode and from 1.7×10^{14} to 1.0×10^{15} cm^{-3} in the continuous mode, gas temperatures 670-950 K in the pulse and 630-880 K in the continuous mode, excitation temperatures 3100-4250 K in the pulse and 3500-4280 K in the continuous mode, slopes and intercepts of the calibration lines and limits of detection and a weak effect on the coefficients of determination. All these parameters were measured in three different positions from the sample inlet of the plasma pencil. Most line intensities and the excitation temperature decreased while calcium lines and rotational temperature calculated from OH radicals increased in the pulsed mode. These results indicate a strong interaction between calcium species and OH radicals. Analysis of real low mineralized waters showed almost proximity of the yielded results to those obtained by reference ICP-OES.

Introduction

Pulsed plasma sources have high variety of possible applications in the various branches, like source for molecular emission spectrometry [1] and for production of hydrogen and carbon nanotubes [2]. Plasma pencil was used for biological and medical applications, e. g. for sterilization of various objects, bacteria elimination on surfaces by created reactive oxygen species [3], for skin treatment [4, 5] and for feasible underwater cleaning of various objects [6, 7, 8]. A combination of radiofrequency (RF) plasma jet operated in the continual mode and Laser-induced plasma was used for breakdown analysis of complex materials. Aerosol prepared by the ultraviolet laser ablation of target solid material was transferred to the plasma jet for secondary excitation and for analysis. The continual mode could be changed to the pulsed mode using pulses synchronised with the repeating laser frequency [9]. A pencil-type plasma jet driven by pulsed DC voltage and low-frequency AC voltage was applied to plasma-cancer cell interactions [10]. The sine-wave excited plasma causes a lower optical emission and significantly lower discharge current than DC excited plasma features. Gram-positive staphylococcus aureus bacteria were inactivated with better performance by the DC pulse excited plasma [11]. An atmospheric pressure, low-power, pulsed plasma source was tested as a portable molecular emission detector. The average operational power is less than 0.2 W and the detection limit for dimethylsulfoxide is 200 ppb [12]. A user-friendly atmospheric pressure plasma jet device can be used for root canal disinfection [13]. The pulsed RF capacitive discharge can be operated in two different modes: A filamentary mode as a turn into filaments and a glow mode as homogeneous glow discharge [14]. Application of alternative pulsed voltage between two parallel plate electrodes can maintain stable discharging pure nitrogen at atmospheric pressure [15]. Microwave (square-wave) pulsed plasmas in argon, nitrogen and silane at a pressures of 5–50 Pa can be generated by an array of four parallel coaxial microwave guides called Plasmodul (Proc. ISPC 15, Orleans, V (2001) 1853) [16]. A kilohertz excited plasma jet was used for pre-ionization of a pulse-modulated nonequilibrium atmospheric-pressure microwave argon plasma discharge [17]. The pulsed atmospheric argon plasma jet is cold and stable and its electron density is 3.9 times higher than plasma in a comparable sinusoidal jet. The sinusoidally produced argon discharges are prone to thermal runaway instabilities [18]. The increase in the pulse width and pulse frequency causes a depression of the maximum bullet velocity and the optical emission intensity of the plasma jet [19]. The increase in the pulse frequency has not any significant influence on the bullet propagation velocity and on the optical emission of the plasma jet [20]. Two or three plasma bullets, at a particular pulse width, are generated by both positive and negative voltage pulses in the each voltage pulse. The electrode polarity and the charges carried by the bullets have significant effect on the propagation of plasma bullets and on the formation

of multiple bullets [20]. Atmospheric pressure plasma jet sustained by pulsed DC power undergoes some transition within each power cycle [21]. It was found that the DC pulse plasma cycle parameter has the influence on the activation of polycarbonate, polystyrene and polypropylene [22]. The irradiance, the power density, the length of discharge and the possible instantaneous power in the continuous mode are lower than in the pulsed mode [23]. The jet tip becomes sharp and the visible length of the jet increases obviously with the increase of used pulsed voltage [24].

The assignment of this work is a comparison of the behaviour of the plasma pencil operated in a continuous RF 13.56 MHz sine mode and in a pulsed mode realized by a rectangular DC modulating signal.

Experimental

The experimental arrangement was the same as in our previous work [25]. The experimental scheme of the plasma pencil spectra acquisition is in Fig. 1 and the scheme of the optical fibre positioning is in the Fig. 2. The only difference is that the power source 13.56 MHz RF generator Dressler Cesar (China) was operated in two different modes: A continuous RF wave mode without any pulse and a pulsed mode with a symmetrical rectangular modulation frequency 22 kHz and duty cycle 80 % for magnesium or 90 % for the other elements. These modulation parameters provide a very good stability of the discharge [26]. All calibration dependences, electron number densities, rotation and excitation temperatures were measured for these both modes. The investigation of pulsation effects was done by measurements of physical and spectrochemical parameters of the discharge. In the first mentioned case an optical emission diagnostics of the plasma is a very frequent approach. Herein the following parameters were measured: Gas temperature (T_g) from Boltzmann plots of rotational lines ($Q_1 1$–$Q_1 9$) of OH spectra, excitation temperature (T_e) from a set of argon atomic lines (603.21, 667.73, 675.28, 687.13 and 714.70 nm) and electron number density (N_e) from H_β line Stark broadening yielded from the fitting the line intensity profile by the Voigt function [25, 27, 28].

Results and discussion

First experimental study concerns the physical parameters (Figs.-5). The experimental results reveal that the temperatures and electron number densities show different response on the pulsed mode and on the continuous mode in the positions 6–8 cm and nearly similar response for the other positions (Figs. 3–5). These measurements were realized with presence of pure water aerosol without the presence of other elements because previous studies did not reveal any significant difference between pure water and water with element addition of the concentrations 1, 2, 3, 5, 7, 10, 20, 30, 50, 70 and 100 mg.l^{-1} [25].

The plasma emission cannot be properly collected in the position 7 cm opposite approx. to the ground electrode (Fig. 1) and that is why there was impossible to realize any measurements [25]. Previous studies [27, 28] showed similar values of the measured N_e, T_e and T_g as in this new work.

Error bars from the electron number density calculations are approximately ± 15 %. These values come from the H_β line fitting and deconvolution procedure. The differences between N_e in the pulse and in the continuous mode are insignificant (Fig. 3).

The same axial trends can be observed for N_e, T_g and T_e (Figs. 3-5). Maxima for all these parameters can be found around the positions 3-4 cm from the sample inlet. These maxima correspond to the proximity of the power electrode and an intensive energy coupling. Despite this fact the measured lines show maximum at the position 8 cm from the sample inlet except for calcium (Fig. 7). The reason is likely that the sample needs a sufficiently long time and path of migration in the discharge column for its atomisation, excitation and ionisation. Around the maximum lines emission at the position 8 cm from the sample inlet (Fig. 6) N_e and T_e are lower in the pulsed mode than in the continuous mode (Figs. 3 and 5). These parameters then make the lines emission lower in the pulsed mode than in the continuous mode. As the relation between the discharge temperature and the lines intensities is rather exponential the observed small changes of the temperatures between the pulsed and the continuous mode provoke significantly higher differences between the lines intensities yielded in the pulsed and in the continuous mode. The difference between rotational temperatures is significant around the detector position 3 cm, which is in the point of maximum T_g, but in the position optimal for the strongest lines emission and signal-to-background ratio (S/B) (highest net intensities at a constant background) is the difference again insignificant (Fig. 4). Comparing the T_e and T_g it can be concluded that the non-isothermic character of the discharge is even intensified in the pulsed mode.

The other part of our study is more focused on effects of pulsation on the selected elements lines intensities. Maximum of these nearly identical measured profiles is at the position 7.5 cm from the aerosol inlet (Figs. 1, 6). Detectable intensities were measured in the region even near the sample inlet. Remarkable intensities are measurable from about 2 cm behind the sample inlet (Fig. 6). The lines intensities corrected to the background are generally higher for the continuous mode than for the pulsed mode except for calcium. The differences between line intensities are significant with respect to error bars for the positions 3–8 cm except for calcium and for the positions from 2 to 6 cm for calcium (Fig. 6).

The calibration dependences constructed for sufficiently intensive lines were measured for pure water as a blank and the concentrations of 1, 2, 3, 5, 7, 10, 20, 30, 50, 70 and 100 mg.l^{-1}. Parameters of the calibration dependences are in Tabs. 1-8.

3–sigma Limit of Detection (LOD) was calculated for each line. The slope was taken from linear regression of the concentration interval 0–10 mg.l^{-1}. 10 successive measurements of the background intensity on the spot of the line maximum for zero concentration were used for calculation of the standard deviation (SD) of the background.

The signal-to-background (S/B) ratio is another important parameter independent on the background noise. It is stable for given experimental conditions. It can be then concluded that the S/B ratio is directly proportional to the depicted and tabulated intensities. The Figs. 6-8 can be depicted either as net intensities or S/B. The presentation is equivalent and independent on the background noise which substantially affects LOD. Therefore the

presented LOD is less reliable indicator.

The pulse mode causes in most cases decrease of the slopes, intercepts, coefficients of determination (R^2) and increase of detection limits (Tabs. 1-8). The exception is calcium and copper (Tabs. 5, 6). The same behaviour is showed by copper also in the axial observation mode.

As an example axial measurements of copper line intensities were also done (Fig. 7). The entrance aperture of the optical bundle was protected from the plasma gases with a piece of a quartz glass located in front of the discharge tip in a distance of about 3 cm [25]. The axial lines intensities are in this case significantly weaker than those taken from the optimal lateral position (Fig. 7). The sensitivity is 5 times worse, too (Tabs. 6, 7). The polynomial character in Fig. 7 is evidentially brought about by the self-absorption throughout the discharge column. It is interesting to highlight that the relative decrease of the intensities in the pulse mode against the continuous mode is directly proportional to the copper concentration. This behaviour is analogical to the lateral mode with linear relation between the intensity and concentration or S/B and concentration. It demonstrates itself by the change of the slope. Even it is not simple to compare nonlinear trends it is evident that the vertical distances between intensity points measured in the continuous and the pulse mode are constant. This is the case of the similar intensities for the concentrations 50-70 $mg.l^{-1}$ (Fig. 7). It can be then concluded that the self-absorption depends on the copper concentration but not on the mode of operation. The self-absorption is always present in such discharge but it is consistent in the lateral mode of spectra acquisition – it does not distort the intensity measurements by remarkable nonlinearity as in the axial mode.

Next experiments were dedicated to the investigation of the relations among the pulse parameters and the measured lines intensities.

The dependence of the S/B on the duty cycle of 65–100 % at the constant modulating frequency of 22 kHz is demonstrated on an example of 3 selected lines in Fig. 8. It was a problem to measure the spectra for magnesium and zinc for the duty cycle of 65 % or less and also for the modulation frequency of 6 or 4 kHz or less because of a high instability and self-switching of the discharge. The other lines show analogical behaviour as magnesium and lithium but the different trend was measured for calcium ionic lines (Fig. 8). The dependence of the S/B or signal intensity on the modulating frequency of 4–22 kHz (Fig. 9) is not monotonous and is probably caused by small changes of the discharge length and demonstrated by visible longitudinal vibrations and total shortening of the discharge. The discharge stability was evaluated by observing the discharge after each change of the modulation frequency and of the duty cycle [26]. The discharge length was measured as a distance between the centre of the power electrode on the right side and discharge tail on the left side and depends on the duty cycle and on the modulation frequency. Identical lengths for 3 modulation frequencies reflect an observation error coming from the length resolution of about 1 mm. The shortest length 10.7 cm was measured for the duty cycle of 65 % and for the modulation frequency of 22 kHz and the longest length of 13.7 cm was measured for the continuum. The background intensity signal is approximately the same for all the modulation frequencies. The opposite behaviour of the Ca lines in the axial profile (Fig. 6) and different dependence on the duty cycle and modulation frequency is likely a consequence of a strong interaction of Ca atoms and ions with OH radicals in the shorter observation positions closer to the sample inlet [29]. This hypothesis is supported by the lateral profiles of the gas temperature from the lines of OH (Fig. 4) in the pulsed and in the continuous mode. This profile well corresponds with that of the Ca ionic lines and also the T_g is higher in the pulsed mode while the T_e shows the opposite behaviour. Similar dependence on the mode parameters is also shown for the Ca atomic line, which *i)* is more intensive under the pulsed mode, *ii)* has analogical axial profile as the ionic lines and the atomic lines of easily ionisable elements (Fig. 6). Also the profiles of the Mg ionic lines are similar to the sodium atomic lines while the Mg atomic line is rather closer to the Cu and Zn lines. The presented calcium lines can be measured with much higher sensitivity in a shorter position from the sample inlet and in the pulsed mode in contrast to any other line.

To show shortly the applicability of the plasma pencil a few real samples have been measured. Five low mineralized commercial natural waters have been selected in order to avoid possible matrix effects (Tab. 9). The results have been verified by comparative measurements with an ICP-OES spectrometer Thermo iCAP 6500 Duo at our laboratory. For the measurements with the both plasma pencil and ICP-OES the same calibration solutions based on Astasol commercial standards [25] were used. Each 50ml flask of a standard or water sample was acidified with 1 ml of 65% nitric acid (p.a. quality). The results show that there are systematic differences between the pulsed mode for 22 kHz and 90 % duty cycle and the continuous mode. The continuous mode brings systematically lower values which are however closer to the ICP-OES results. The explanation lies behind this preliminary academic study of the pulsed mode and the potential use of the plasma pencil should be verified by upcoming research of the pulsed mode (reaction kinetics). The confidence intervals were constructed under the Dean-Dixon method for 5 replicates at the probability of 95 %. Even the yielded results from the continuous mode and the pulsed mode of the pencil and from the pencil and the ICP-OES are significantly different the differences are almost within usual range when one sample is analysed by several laboratories.

Conclusions

The study of the pulsed mode shows that the signal intensities are obviously lower for the pulsed mode than for the continuous one. The effect of the pulsed mode depends on the selected line. Calcium most intensive ionic lines 393 and 396 nm are significantly stronger in the pulsed mode than in the continuous one. The explanation is not simple but it can be apparently related to the different axial profiles of these lines. It can be attributed to the oxide or hydroxide formation and dissociation in shorter distances from the sample inlet. Most lines increase with the increasing duty cycle and the decreasing pulse frequency while those of Ca decrease. The effect of pulsation switches off and shortens the discharge. This mode of operation worsens the excitation capabilities but apparently changes the energy distribution towards the OH radicals thus leading to the increase

of the rotational temperature, decrease of the excitation temperature and the enhanced emission of the calcium ionic lines (393.347, 396.827) and the atomic line (422.657 nm).

The analysis of low mineralized water samples showed that the pulsed mode almost yields results more similar to the reference ICP-OES measurement. This fact will be subject of further studies behind these preliminary pulsation experiments.

Acknowledgements

This work was supported by the projects CEITEC – Central European Institute of Technology (CZ.1.05/1.1.00/02.0068) and CEPLANT – R&D Center for Low-Cost Plasma and Nanotechnology Surface Modifications (CZ.1.05/2.1.00/03.0086) from European Regional Development Fund.

References

1. Z. Jin, Y. Su, Y.Duan, *Anal. Chem.* 2001, **73**, 360-365.
2. L. N. Mishra, K. Shibata, H. Ito, N. Yugami, Y. Nishida, *Surf. Coatings Technol.,* 2007, **201**, 6101-6104.
3. M. Laroussi, C. Tendero, X. Lu, S. Alla, W. L. Hynes, *Plasma Process. Polym.*, 2006, **3**, 470–473.
4. M. Larousi, *IEEE Transactions on Plasma Sci.*, 2008, **36**, 1298-1299.
5. M. Laroussi and X. Lu, *Appl. Phys. Lett.*, 2005, **87**, p. 113 902.
6. J. Janča, M. Klíma, P. Slavíček, L. Zajíčková, *Surf. Coatings Technol.*, 1999, **116–119**, 547–551.
7. M. Klíma, P. Slavíček, L. Zajíčková, J. Janča, *Czechoslov. J. Phys.*, 1999, 49, 321-328.
8. M. Klíma, P. Slavíček, M. Šíra, T. Čižmár, P. Vaněk, *Czechoslov. J. Phys.*, 2006**, 56/B**, 1051-1056.
9. J. D. Pedarnig, J. Heitz, E. R. Ionita, G. Dinescu, B. Praher, R. Viskup, *Appl. Surf. Sci.,* 2011, **257,** 5452-5455, DOI: 10.1016/j.apsusc.2010.11.112.
10. H. M. Joh, S. J. Kim, T. H. Chung, S. H. Leeem, *AIP Advances*, 2013, **3**, 092128, DOI: 10.1063/1.4823484.
11. Q. Xiong. X. P. Lu, K. Ostrikov. Y. Xian, C. Zou, Z. Xiong, Y. Pan, *Phys. of Plasmas*, 2010, **17**, 043506, DOI: 10.1063/1.3381132.
12. Z. Jin, Y. Su, Y. Duan, *Anal. Chem*, 2001, **73**, 360-365.
13. Y. Xian, X. Lu, Z. Tang, Q. Xiong, W. Gong, D. Liu, Z. Jiang, Y. Pan, *J. Appl. Phys.*, 2010, **107**, 063308, DOI: 10.1063/1.3360932.
14. N. Balcon, A. Aanesland, R. Boswell, *Plasma Sources Sci. Technol.*, 2007, **16**, 217-225.
15. R. Hayakawa, T. Yoshimura, A. Ashida, N. Fujimura, H. Kitahata, M. Yuasa, *J. Appl. Phys.,* 2004, Vol. 96, No. 11, 6094-6096
16. J. Kruger, T. Kubach, J. Feichtinger, K. Hirsch, P. Lindner, S. Quell, A. Schulz, R. Stirn, M. Walker, U. Schumacher, *Surf. Coatings Technol.*, 2003, **174-175**, 933-937.
17. S. Li, M. Xu, X. Zhang, J. Zhang, *Appl. Phys. Lett.*, 2012, **100**, 174101, DOI: 10.1063/1.4705433.
18. J. L. Walsh, M. G. Kong, A*ppl. Phys. Lett.*, 2007, **91**, 221502.
19. Q. Xiong, X. Lu, Y. Xian, J. Liu, C. Zou, Z. Xiong, W. Gong, K. Chen, X. Pei, F. Zou, J. Hu, Z. Jiang, Y. Pan, *J. Appl. Phys.*, 2010, **107**, 073302, DOI: 10.1063/1.3369538.
20. Y. Xian. X. Lu, J. Liu, S. Wu, D. Liu, Y. Pan, *Plasma Sources Sci. Technol.*, 2012, **21**, 034013 (6pp), DOI: 10.1088/0963-0252/21/3/034013.
21. C. Hsu, C. Wu, C. Chen, W. Cheng, *Jpn. J. Appl. Phys.*, 2009, **48**, 076002, DOI: 10.1143/JJAP.48.076002.
22. D. P. Dowling, F. T. O'Neill, S. J. Langlais, V. J. Law, *Plasma Proces. Polym.*, 2011, **8**, p. 718-727, DOI: 10.1002/ppap.201000145.
23. S. Hofmann, P. Bruggeman, *IEEE Transactions on Plasma Sci.*, 2011, Vol. 39, No. 11, p. 2332-2333.
24. Z. Niu, T. Shao, C. Zhang, H. Jiang, C. Li, G. Wang, J. Tan, P. Yan, *IEEE Transactions on Plasma Sci*, Vol. 39, No. 11, p. 2322-2323.
25. L. Novosád, A. Hrdlička, P. Slavíček, V. Otruba, V. Kanický, *J. Anal. At. Spectrom.*, 2012, **27,** 305-309, DOI: 10.1039/c1ja10278h.
26. P. Slavíček, D. Skácelová, *IEEE Transactions on Plasma Sci*, 2012, Vol. 40, No. 11, p. 2920-2924, ISSN 0093-3813, DOI: 10.1109/TPS.2012.2213275.
27. P. Slavíček, V. Buršíková, A. Brablec, V. Kapička, M. Klíma, *Czechoslov. J. Phys.*, 2004**, 54/C**, 586-591.
28. P. Slavíček, M. Klíma, J. Janča, A. Brablec, J. Kadlecová, P. Smékal, *Czechoslov. J. Phys.*, 2006, **56**/**B**, B1057-B1061.
29. T. Frentiu, M. Ponta, E. Darvasi, M. Frentiu, E. A. Cordos, *Acta. Chim. Slov.,* 2010, **57**, 173-181.

Notes and references

[a] *Masaryk University, Faculty of Science, Department of Chemistry, Kotlářská 2, 61137 Brno, Czech Republic, e-mail: 78105@mail.muni.cz*
[b] *Masaryk University, Central European Institute of Technology (CEITEC MU), Kamenice 753/5, 62500 Brno, Czech Republic, e-mail: ahrdlicka@chemi.muni.cz, ales2003h@centrum.cz*
[c] *Masaryk University, Faculty of Science, Department of Physical Electronics, Kotlářská 2, 61137 Brno, Czech Republic, e-mail:ps94@sci.muni.cz*

Figures and tables

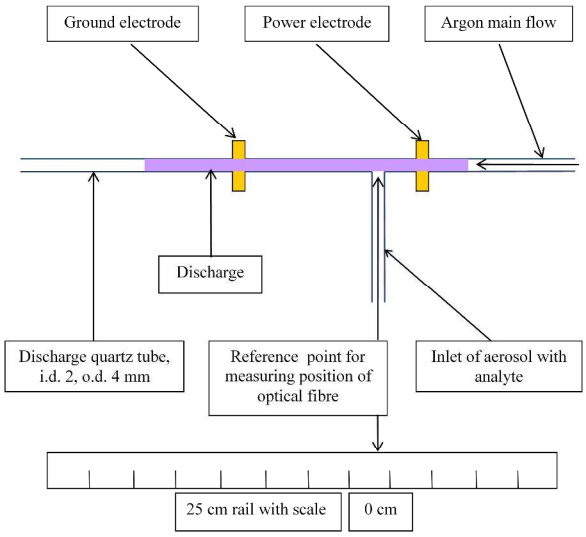

Figure 1: Experimental scheme of plasma pencil spectra acquisition.

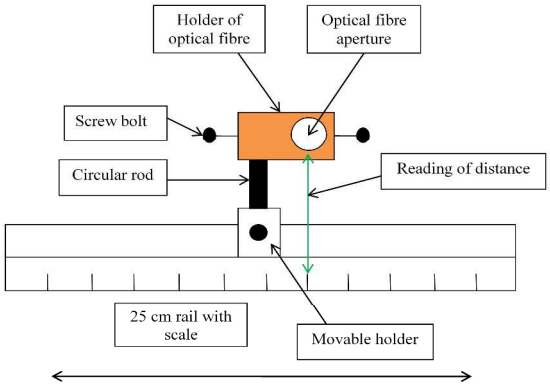

Figure 2: Scheme of the optical fibre positioning.

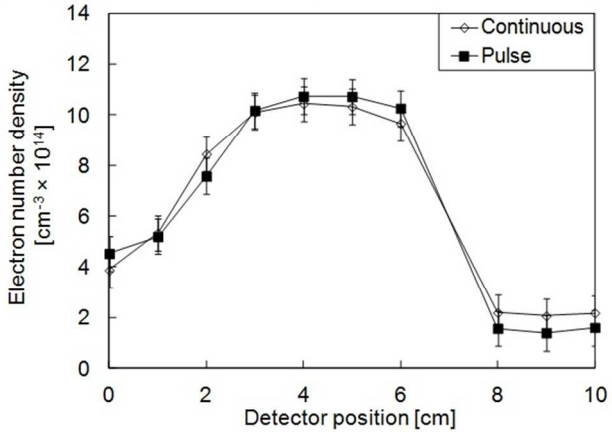

Figure 3: Electron number density profile from the H beta line along the discharge axis for the continuous mode and pulsed mode.

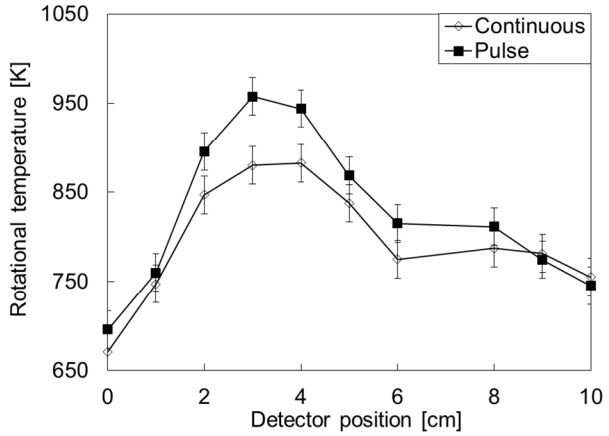

Figure 4: Gas temperature profile from the OH lines along the discharge axis for both modes.

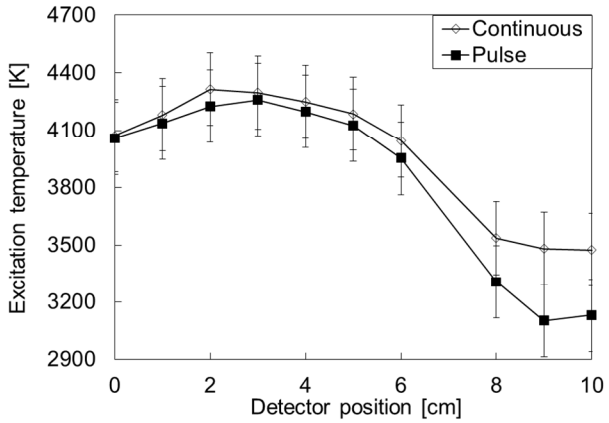

Figure 5: Excitation temperature profile from the argon lines for both modes.

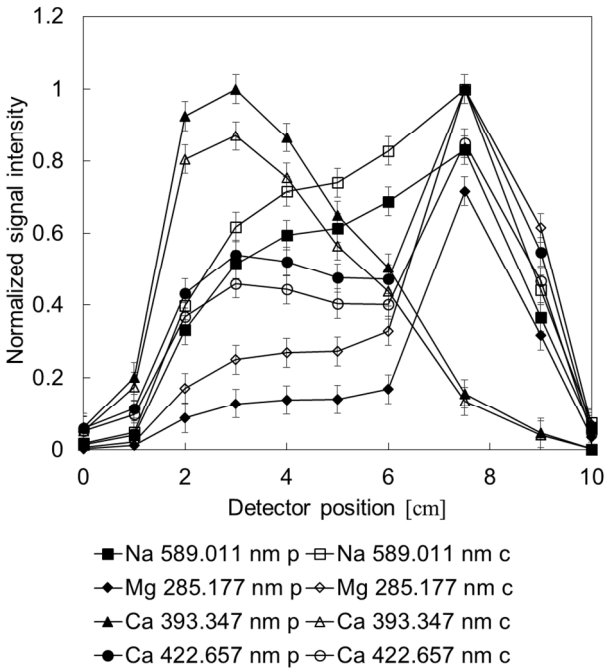

Figure 6: Dependences of normalized signal intensities of sodium, magnesium and calcium on the detector position from 0 to 10 cm, where p is pulsed mode and c is continuous mode.

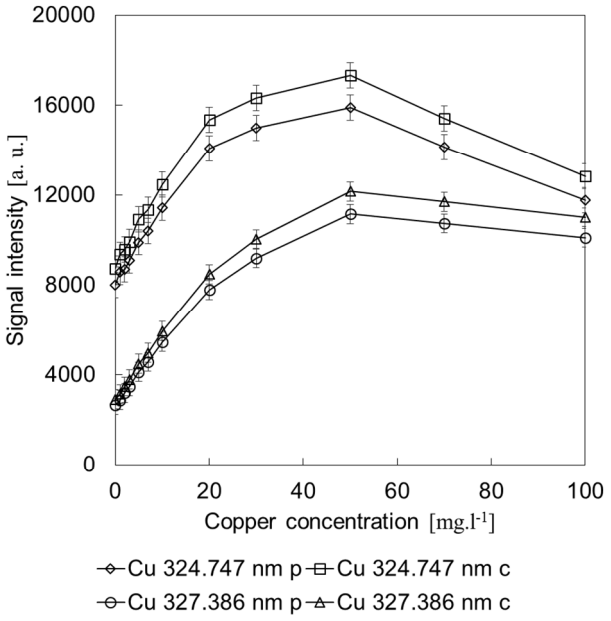

Figure 7: Calibration dependences for copper in pulsed mode p and in the continuous mode c in axial position.

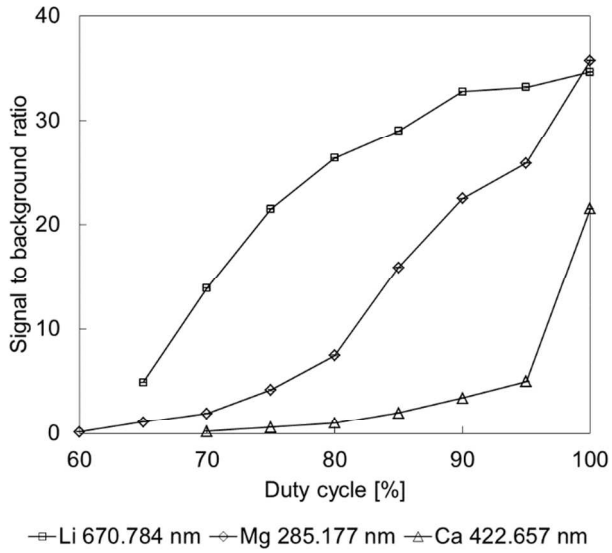

Figure 8: Dependences of signal-to- background ratio on the duty cycle for lithium, magnesium and calcium at the constant modulation frequency of 22 kHz.

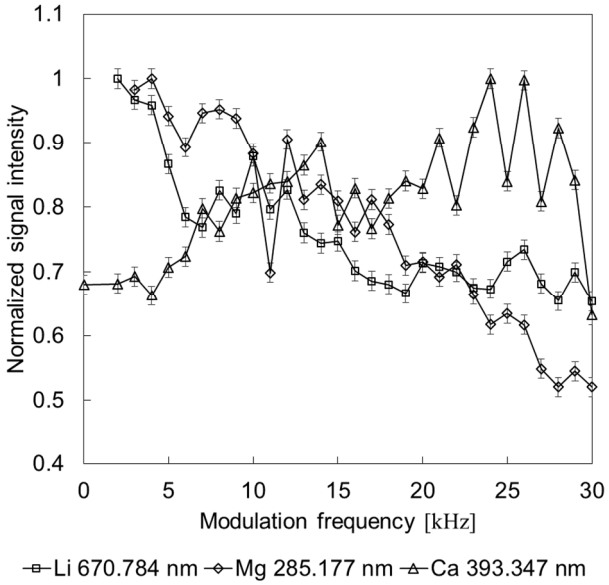

Figure 9: Dependences of normalized signal intensities on the modulation frequency for lithium, magnesium and calcium at the constant duty cycle of 90 %.

Table 1: Calibration data for lithium for both modes, integration time 0.5 s, width of spectrometer entrance slit 16 µm. 5 replicates were done for all the intensities measurements except for blank which was measured 10 times.

Detector position [cm]	Wavelength [nm]	Linear regression Slope	Linear regression Intercept	R^2	Detection limit [$mg.l^{-1}$]	S/B ratio for 100 $mg.l^{-1}$
Pulsed mode						
9	610.359	16.127	3572.8	0.994	3.67	3.887
9	610.784	812.75	3328.5	0.968	0.05	3.750
8	610.359	23.749	3580	0.993	2.63	7.939
8	670.784	1097.4	3372	0.988	0.05	8.539
6	610.359	7.1082	3538.4	0.987	3.76	2.857
6	670.784	642.38	3359.1	0.999	0.02	4.598
Continuous mode						
9	610.359	17.158	3547.2	0.967	3.25	3.561
9	670.784	872.14	3367.9	0.997	0.03	4.053
8	610.359	25.039	3512.7	0.980	2.38	8.574
8	670.784	1202.5	3352.6	0.983	0.03	9.911
6	610.359	8.2836	3590.1	0.968	3.36	3.048
6	670.784	682.61	3304.5	0.994	0.01	4.793

Table 2: Calibration data for sodium for both modes, integration time 3 s, width of spectrometer entrance slit 16 µm.

Detector position [cm]	Wavelength [nm]	Linear regression Slope	Linear regression Intercept	R^2	Detection limit [$mg.l^{-1}$]	S/B ratio for 100 $mg.l^{-1}$
Pulsed mode						
9	589	472.16	3842.5	0.994	0.15	3.753
9	589.597	474.25	3726.4	0.998	0.12	2.971
8	589	663.34	4827.2	0.999	0.16	9.454
8	589.597	742.53	4793.8	0.998	0.18	7.533
6	589	985.72	4357.1	0.996	0.06	7.701
6	589.597	837.81	5307.3	0.999	0.19	6.178
Continuous mode						
9	589	586.15	4498.6	0.993	0.08	4.715
9	589.597	316.26	3872.4	0.999	0.17	3.850
8	589	784.85	6292.7	0.990	0.10	11.469
8	589.597	386.27	4829	0.997	0.35	9.432
6	589	1192	5408.3	0.997	0.04	9.582
6	589.597	594.52	4101.8	0.992	0.36	7.964

Table 3: Calibration data for magnesium for both modes, width of spectrometer entrance slit 24 µm.

Detector position [cm]	Integration time [s]	Wavelength [nm]	Linear regression Slope	Linear regression Intercept	R^2	Detection limit [$mg.l^{-1}$]	S/B ratio for 100 $mg.l^{-1}$
Pulsed mode							
9	10	279.519	159.13	3147.2	0.987	0.21	5.212
	10	280.257	65.547	4376.9	0.995	0.67	1.331
	5	285.177	384.85	2039.5	0.992	0.07	24.945

	10	279.519	615	3918.4	0.999	0.07	14.720
8	10	280.257	349.5	4235	0.999	0.18	7.920
	5	285.177	695.42	1905.1	0.999	0.06	38.963
	10	279.519	351.52	6407.3	0.997	0.32	5.592
6	10	280.257	193.84	6618.9	0.999	0.36	3.021
	5	285.177	324.49	3653.2	0.999	0.15	9.616
Continuous mode							
	10	279.519	211.62	4165.8	0.999	0.02	7.463
9	10	280.257	86.21	5894.6	0.999	0.63	2.142
	5	285.177	490.52	2604	0.987	0.06	34.064
	10	279.519	786.4	5139.4	0.999	0.06	20.581
8	10	280.257	455.83	5547	0.998	0.15	11.939
	5	285.177	904.18	2632.5	0.996	0.05	53.549
	10	279.519	495.37	9103.4	0.989	0.24	8.812
6	10	280.257	270.46	9215.3	0.997	0.27	4.598
	5	285.177	458.97	5048	0.995	0.13	13.575

Table 5: Calibration data for calcium for both modes, integration time 5 s, width of spectrometer entrance slit 24 μm.

Pulsed mode						
Detector position [cm]	Wavelength [nm]	Linear regression		R^2	Detection limit [$mg.l^{-1}$]	S/B ratio for 100 $mg.l^{-1}$
		Slope	Intercept			
	393.347	18.32	1798.3	0.972	0.52	0.883
9	396.827	11.583	1764.5	0.972	1.54	0.553
	422.657	201.4	2137	0.985	0.12	10.849
	393.347	83.475	2382.7	0.993	0.36	3.615
8	396.827	49.357	2280.4	0.993	0.32	2.185
	422.657	341.28	2836.1	0.992	0.07	16.624
	393.347	591.12	5702.6	0.996	0.08	10.395
6	396.827	352.64	5874.8	0.995	0.17	5.926
	422.657	386.91	5891	0.997	0.09	6.861
Continuous mode						
	393.347	15.631	1442.6	0.974	0.57	0.591
9	396.827	9.0547	1475.2	0.976	1.58	0.315
	422.657	174.58	1883.7	0.992	0.17	8.935
	393.347	72.516	1916.4	0.987	0.39	2.786
8	396.827	43.974	1874.5	0.989	0.41	1.576
	422.657	291.38	2401.3	0.993	0.07	13.408
	393.347	502.63	4953.9	0.989	0.08	8.752
6	396.827	298.35	4738.5	0.992	0.21	4.718
	422.657	335.16	5138.2	0.991	0.09	5.306

[5]

Table 6: Calibration data for copper for both modes, integration time 0.35 s, width of spectrometer entrance slit 16 μm.

Pulsed mode						
Detector position [cm]	Wavelength [nm]	Linear regression		R^2	Detection limit [$mg.l^{-1}$]	S/B ratio for 100 $mg.l^{-1}$
		Slope	Intercept			
9	324.742	352.06	2362.1	0.997	0.19	11.816
9	327.381	243.16	1195.4	0.996	0.09	17.153
8	324.742	857.37	5614.6	0.999	0.04	13.023

8	327.381	558.29	3192.5	0.993	0.05	16.899
6	324.742	252.03	6509.2	0.994	0.17	3.879
6	327.381	176.13	1793.8	0.999	0.12	9.754
			Continuous mode			
9	324.742	319.27	2135.2	0.997	0.20	10.604
9	327.381	217.36	990.25	0.996	0.09	14.156
8	324.742	778.92	4893.6	0.997	0.05	11.840
8	327.381	501.27	2867.4	0.998	0.05	13.035
6	324.742	232.64	5872.3	0.999	0.14	3.423
6	327.381	161.35	1582.9	0.995	0.16	8.043

Table 7: Calibration data for copper in the discharge axis for both modes, integration time 0.35 s, width of spectrometer entrance slit 16 μm.

Mode type	Wavelength [nm]	Polynomial regression	R^2	Detection limit [mg.l^{-1}]	S/B ratio for 100 mg.l^{-1}
continuous	324.742	$y = 0.021x^3 - 5.2674x^2 + 324.57x + 6194.1$	0.995	0.13	0.319
	327.381	$y = 0.0132x^3 - 3.3829x^2 + 254.28x + 1895$	0.998	0.15	2.158
pulse	324.742	$y = 0.0247x^3 - 5.8342x^2 + 358.42x + 6872$	0.994	0.09	0.471
	327.381	$y = 0.0138x^3 - 3.7641x^2 + 283.25x + 2125$	0.996	0.09	2.792

Table 8: Calibration data for zinc for both modes, wavelength 213.861 nm, integration time 10 s, width of spectrometer entrance slit 40 μm.

Detector position [cm]	Mode type	Linear regression		R^2	Detection limit [mg.l^{-1}]	S/B ratio for 100 mg.l^{-1}
		Slope	Intercept			
9	pulse	69.507	1285.6	0.986	1.52	3.331
9	continuous	104.26	1764.2	0.996	1.03	5.544
8	pulse	130.18	1382.5	0.995	1.48	7.112
8	continuous	195.27	1547.3	0.985	1.26	11.058
6	pulse	36.767	1628.4	0.993	1.01	1.291
6	continuous	55.151	1483.8	0.997	1.37	2.314

Table 9: Determination of selected elements in commercial low mineralized drinkable waters

Element	Magnesium				Calcium				Sodium			
Wavelength [nm]	279.536		280.25		396.4		396.84		589		589.6	
Mode	cont.	pulse	cont.	pulse	cont.	pulse	cont.	pulse	cont.	pulse	cont.	pulse
					Results for plasma pencil							
Sample name	Element concentration [mg.l^{-1}]											
Izvorul Minunilor	4.36	4.073	4.132	3.660	23.5	15.51	24.82	16.69	1.959	1.079	2.009	0.897
Cristaline Metzeral	2.576	1.525	4.113	1.712	4.277	3.388	6.090	4.595	1.927	0.921	1.973	0.787

Good Water	8.47	7.919	9.14	9.063	6.720	6.071	6.858	8.037	14.829	14.864	15.348	11.981
Toma Natura	10.17	12.59	10.04	14.38	37.6	41.52	38.07	39.63	1.419	1.252	1.351	1.061
Potable water in Brno city	4.548	4.158	4.374	5.011	91.8	95.7	96.9	89.6	3.942	2.083	3.983	1.729
					Confidence interval [mg.l^{-1}]							
Izvorul Minunilor	0.11	0.095	0.098	0.064	1.0	0.57	0.37	0.28	0.032	0.021	0.023	0.012
Cristaline Metzeral	0.085	0.021	0.036	0.025	0.031	0.029	0.045	0.016	0.019	0.019	0.035	0.087
Good Water	0.15	0.037	0.11	0.099	0.049	0.041	0.031	0.037	0.075	0.025	0.019	0.012
Toma Natura	0.14	0.15	0.11	0.12	1.1	0.36	0.22	0.70	0.032	0.056	0.071	0.051
Potable water in Brno city	0.032	0.037	0.035	0.028	1.0	1.0	1.2	1.2	0.048	0.052	0.082	0.042

			Results for ICP-OES Element concentration [mg.l^{-1}]			
Izvorul Minunilor	4.362	3.911	16.99	16.04	1.178	1.195
Cristaline Metzeral	1.787	1.599	5.855	5.248	3.771	3.762
Good Water	9.824	9.127	6.204	5.619	10.96	10.84
Toma Natura	8.11	7.555	29.65	28.83	1.060	1.057
Potable water in Brno city	4.349	3.9	97.88	92.81	3.404	3.376
			Confidence interval [mg.l^{-1}]			
Izvorul Minunilor	0.011	0.001	0.044	0.026	0.0044	0.0050
Cristaline Metzeral	0.002	0.004	0.028	0.024	0.012	0.019
Good Water	0.043	0.025	0.007	0.020	0.050	0.037
Toma Natura	0.053	0.007	0.025	0.084	0.0090	0.0010
Potable water in Brno city	0.004	0.014	0.17	0.58	0.022	0.023